
L2G-Net: Local to Global Spectral Graph Neural Networks via Cauchy Factorizations

Samuel Fernández-Menduiña¹ Eduardo Pavez¹ Antonio Ortega¹

Abstract

Despite their theoretical advantages, spectral methods based on the graph Fourier transform (GFT) are seldom used in graph neural networks (GNNs) due to the cost of computing the eigenbasis and the lack of vertex-domain locality in spectral representations. As a result, most GNNs rely on local approximations such as polynomial Laplacian filters or message passing, which limit their ability to model long-range dependencies. In this paper, we introduce a novel factorization of the GFT into operators acting on subgraphs, which are then combined via a sequence of Cauchy matrices. We use this factorization to propose a new class of spectral GNNs, which we term L2G-Net (Local-to-Global Net). Unlike existing spectral methods, which are either fully global (when they use the GFT) or local (when they use polynomial filters), L2G-Net operates by processing the spectral representations of subgraphs and then combining them via structured matrices. Our algorithm avoids full eigendecompositions, exploiting graph topology to construct the factorization with quadratic complexity in the number of nodes, scaled by the subgraph interface size. Experiments on benchmarks stressing non-local dependencies show that L2G-Net outperforms existing spectral techniques and is competitive with the state-of-the-art with orders of magnitude fewer learnable parameters.

1. Introduction

Spectral graph methods exploit the eigenvectors of the graph Laplacian (Chung, 1997) to process signals defined over irregular domains. They are central for applications such as spectral graph neural networks (GNNs) (Bruna et al., 2014). Drawing an analogy with signal processing in regular domains (Ortega et al., 2018), the transformation

that projects signals onto the Laplacian eigenbasis \mathbf{U} is often called the graph Fourier transform (GFT), and among other properties, it provides a representation that captures global structural properties of the graph.

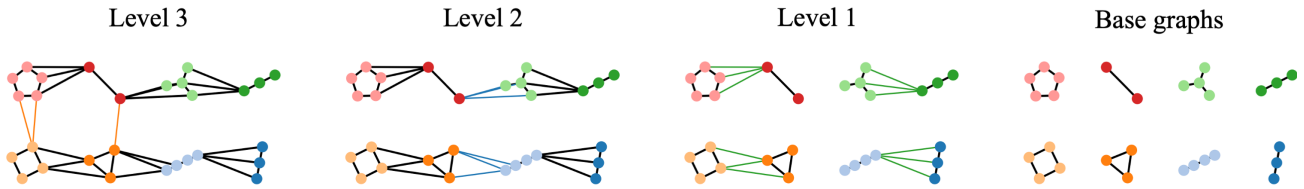
Despite using well-defined graph signal frequencies, GFT-based GNNs are far less used in practice than polynomial spectral filters (Defferrard et al., 2016; Levie et al., 2018; He et al., 2021) or message-passing neural networks (MPNNs) (Kipf and Welling, 2017). This can be attributed to two limitations: 1) the complexity of computing the full Laplacian eigenbasis (the GFT) is cubic in the number of nodes, rendering exact spectral methods impractical for large graphs (Bronstein et al., 2017), and 2) GFT-domain operations are generally global in the vertex domain, i.e., modifying a single spectral coefficient can affect all nodes simultaneously (Ortega et al., 2018). While global modeling may help capture long-range dependencies (Dwivedi et al., 2022), spectral GNNs are less effective at modeling local vertex domain inductive biases that can benefit some graph machine learning tasks (Alon and Yahav, 2020).

Polynomial approximations and MPNNs replace global GFT operations with repeated sparse matrix multiplications with a graph operator (e.g., the adjacency or the graph Laplacian) (Kipf and Welling, 2017) or a learned higher order polynomial of the operator (Defferrard et al., 2016). These approaches are computationally efficient and induce a k -hop locality bias, which partially explains their empirical success on homophilic graphs (Hariri et al., 2025). However, modeling long-range dependencies with local operators typically requires multiple message-passing steps, often leading to oversquashing (Alon and Yahav, 2020) and optimization instabilities (Arroyo et al., 2025). Replacing the Laplacian with a higher-order polynomial of the Laplacian may alleviate these issues, but often at the cost of numerical instability or restrictive parameter constraints (Hariri et al., 2025). Combining global and local information via attention (Deng et al., 2024) typically requires many more learnable parameters, and potentially sacrifices graph-domain interpretability (cf. Section 2.3).

In this paper, we introduce a new class of spectral GNNs that builds *global* spectral representations by aggregating *local* spectral coefficients. Our basic idea is illustrated in

¹University of Southern California. Correspondence to: Samuel Fernández-Menduiña <samuelf9@usc.edu>.

(a) A hierarchical graph



(b) Spectral processing in L2G-Net

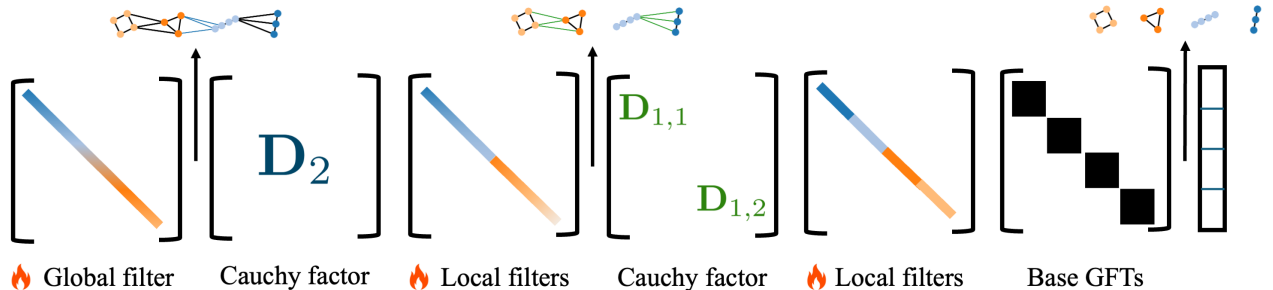


Figure 1. (a) A graph in $\mathcal{F}(L = 3, \{\mathcal{G}_i\}_{i=1}^S, k = 3)$. Bridge edges are shown in different colors. The GFT basis of the final graph can be expressed as the product of the stack of GFT bases of the base graphs by a sequence of Cauchy factors. (b) We first compute the base GFTs of small subgraphs (right) and apply local spectral filters. We mix the outputs via Cauchy factors corresponding to bridge edges. After all hierarchical merges, a global spectral filter acts on the full graph representation (left). This allows for global filtering that preserves locality while avoiding full eigendecompositions.

Figure 1. We first demonstrate that any GFT can be *exactly factorized* into a sequence of localized transformations. Specifically, given a graph partition (Figure 1 (a)), we show that the GFT admits a hierarchical decomposition into the GFTs of the local *subgraphs*, each a connected set of nodes forming the partition, which are then multiplied by a series of *Cauchy matrices*, each arising from rank-one updates associated with an edge connecting two subgraphs (cf. Figure 1). We call an *interface* the set of edges connecting two subgraphs. Matrices in the Cauchy factorization are block-diagonal, which makes them localized to regions of the graph corresponding to these blocks, while the composition of these blocks recovers the global GFT.

This factorization yields a divide-and-conquer strategy that allows us to define Local-to-Global Net (L2G-Net), a new type of spectral GNN. As shown in Figure 1, at each stage, the outputs of each localized GFT (each representing spectral information for the corresponding subgraph) are processed using learnable filters before they are merged using Cauchy factors. In the last level, a global learnable spectral filter processes the entire signal without requiring a full eigendecomposition of the global Laplacian (cf. Figure 1 (b)). L2G-Net combines the benefits of global spectral processing while introducing locality biases by construction in the spectral layer. We show that the GFT has a quadratic *factorization cost*, i.e., the complexity of computing all terms of the factorization is quadratic in the number

of nodes, scaled by the size of the subgraph interface. For graphs exhibiting modular or hierarchical structure, common in real-world networks (Barthélemy, 2011; Clauset et al., 2008), this leads to significant computational savings over the full eigendecomposition.

While this complexity result holds for arbitrary graph partitions, the factorization cost may be high if the interface size is large. Hence, we introduce a graph decomposition algorithm that explicitly aims to minimize the cost of computing the Cauchy factorization. Specifically, we seek balanced partitions with small interface sizes, directly optimizing the theoretical factorization cost. This approach also provides an interpretable perspective on GNN processing: the method first operates on densely connected, highly coupled subgraphs and then progressively merges their spectral representations into a global one by exploiting weaker interactions between components. When such favorable partitions are not available, we use spectral sparsification (Spielman and Srivastava, 2008) to reduce the interface size while preserving the spectral properties of the original graph. We validate this analysis through experiments on synthetic graphs, confirming the predicted runtime scaling and demonstrating substantial improvements over dense eigendecomposition of the graph Laplacian

We apply L2G-Net in a transductive benchmark of large-scale graphs (Platonov et al., 2023) emphasizing non-local structural dependencies, where MPNNs are known

to struggle due to their inductive biases (Alon and Yahav, 2020; Rusch et al., 2023; Hariri et al., 2025). Our results show that L2G-Net outperforms existing spectral strategies (Hariri et al., 2025), with lower complexity than applying the global GFT and a similar number of learned parameters. We achieve results competitive with state-of-the-art techniques using attention (Deng et al., 2024), while requiring orders of magnitude fewer learnable parameters.

Our contributions are: 1) we show that the GFT basis admits an exact factorization via Cauchy matrices that works for any possible partition, and we propose a quadratic-time algorithm to compute this factorization directly from the graph Laplacian, without a full eigendecomposition (Section 3), 2) we provide an algorithm to find partitions that are computationally advantageous for computing this Cauchy factorization (Section 4), 3) we introduce L2G-Net, a new family of spectral GNNs based on this factorization that combines localized and global computations (Section 5).

2. Background

Notation. Uppercase and lowercase bold letters, such as \mathbf{A} and \mathbf{a} , denote matrices and vectors, respectively. The n th entry of \mathbf{a} is a_n , and the (i, j) th entry of \mathbf{A} is A_{ij} .

2.1. Spectral graph theory

Let $\mathcal{G} = (\mathcal{V}, \mathcal{E}, \mathbf{W}, \mathbf{V})$ be a weighted undirected graph, with vertex set \mathcal{V} , edge set \mathcal{E} , weighted adjacency matrix \mathbf{W} , and self-loop diagonal matrix \mathbf{V} . The generalized graph Laplacian (GGL) is $\mathbf{L} \doteq \mathbf{D} - \mathbf{W} + \mathbf{V}$, where $\mathbf{D} \doteq \text{diag}(\mathbf{1}^\top \mathbf{W})$ is the degree matrix. Given the eigendecomposition $\mathbf{L} = \mathbf{U} \text{diag}(\boldsymbol{\lambda}) \mathbf{U}^\top$, we refer to \mathbf{U} as the graph Fourier transform (GFT) (Chung, 1997; Ortega et al., 2018) associated with \mathcal{G} . Any graph GGL decomposes into a sum of rank-one terms (or ‘‘baby Laplacians’’), one for each edge contribution.

Proposition 2.1 ((Batson et al., 2014)). *Let \mathbf{e}_j be the j th canonical vector, for $j = 1, \dots, n$. Then, the GGL \mathbf{L} of an undirected graph can be written as*

$$\mathbf{L} = \sum_{(i,j) \in \mathcal{E}, i \neq j} w_{ij} (\mathbf{e}_i - \mathbf{e}_j)(\mathbf{e}_i - \mathbf{e}_j)^\top + \sum_{(i,i) \in \mathcal{E}} v_{ii} \mathbf{e}_i \mathbf{e}_i^\top, \quad (1)$$

where w_{ij} denotes the edge weights, for $i, j = 1, \dots, |\mathcal{V}|$.

We use Proposition 2.1 to express the addition of an edge to a graph with Laplacian \mathbf{L} as a *rank-one update*:

$$\tilde{\mathbf{L}} = \mathbf{L} + w_{ij} \mathbf{v} \mathbf{v}^\top, \quad (2)$$

with $\mathbf{v} = (\mathbf{e}_i - \mathbf{e}_j)$ when adding an edge between i and j .

2.2. Cauchy matrices

Definition 2.1 (Cauchy matrix (Gastinel, 1960)). Given two vectors $\mathbf{x} \in \mathbb{R}^n$ and $\mathbf{y} \in \mathbb{R}^n$ with no common entries, the Cauchy matrix $\bar{\mathbf{C}}(\mathbf{x}, \mathbf{y}) \in \mathbb{R}^{n \times n}$ has entries $\bar{C}_{ij} = 1/(x_i - y_j)$ for $i, j = 1, \dots, n$.

Definition 2.2 (Orthogonal Cauchy-like matrix, OCLM (Fasino, 2023; Cai et al., 2018)). A matrix $\mathbf{C}(\mathbf{x}, \mathbf{y}) \in \mathbb{R}^{n \times n}$ is an orthogonal Cauchy-like matrix if it is orthogonal and can be written as $\mathbf{C}(\mathbf{x}, \mathbf{y}) = \text{diag}(\mathbf{s}) \bar{\mathbf{C}}(\mathbf{x}, \mathbf{y}) \text{diag}(\mathbf{t})$ for some $\mathbf{s}, \mathbf{t} \in \mathbb{R}^n$.

OCLMs relate eigenvectors before and after a rank-one update of a symmetric matrix (Fasino, 2023). Each rank-one update corresponds to an edge in the GGL. In particular, for (2), with $\mathbf{L} = \mathbf{U} \text{diag}(\boldsymbol{\lambda}) \mathbf{U}^\top$ and $\tilde{\mathbf{L}} = \tilde{\mathbf{U}} \text{diag}(\tilde{\boldsymbol{\lambda}}) \tilde{\mathbf{U}}^\top$, it can be shown that (Fernández-Menduiña et al., 2025):

$$\tilde{\mathbf{U}}^\top = -\mathbf{C}(\tilde{\boldsymbol{\lambda}}, \boldsymbol{\lambda}) \mathbf{U}^\top. \quad (3)$$

For rank-one updates, $\tilde{\boldsymbol{\lambda}}$ can be found via the secular equation (Golub, 1973) (cf. Section A). Relation (3) applies only to graphs without repeated eigenvalues and to updates that are not orthogonal to any column of \mathbf{U} (cf. Section C).

2.3. Related work

Graph rewiring and transformers. Several approaches address long-range dependencies by modifying the graph structure or adding attention-based mechanisms. Graph rewiring methods aim to reduce the effective graph diameter (Barbero et al., 2023), while graph transformers model global interactions through attention mechanisms (Deng et al., 2024). However, these approaches often add computational complexity by creating denser graph shift operators or weakening the graph’s topological inductive bias (Hariri et al., 2025) (cf. Section 6.3). In contrast, our Cauchy factorization is exact; potential approximations (spectral sparsification) simplify the computational complexity while providing guarantees on the spectrum of the resulting Laplacian (Spielman and Srivastava, 2008)

Positional encodings. Using Laplacian eigenvectors as node features has been proposed to inject global structural information into MPNNs (Dwivedi and Bresson, 2020; Huang et al., 2023). These methods leverage spectral information as input features rather than as a computational basis. As a result, their ability to exploit the graph’s global properties is limited. In contrast, our work operates directly on the coefficients of local GFTs, and progressively merges them to obtain the full spectral representation.

Deep GNNs and differential equations. Deep architectures (Li et al., 2019) or Neural ODEs (Poli et al., 2019; Chamberlain et al., 2021) can also help expand the receptive field via techniques like residual connections (Chen

et al., 2020). Nonetheless, these methods still rely on local message passing to propagate information; so the receptive field grows at most linearly with depth, often requiring hundreds of layers to capture long-range interactions. In contrast, our hierarchical spectral framework decouples the receptive field from depth. This allows the architecture to focus on learning complex feature transformations without the signal degradation or over-smoothing issues (Rusch et al., 2023) typical of vertex-domain propagation.

Fast algorithms for GFTs. Early works proposed approximating the Laplacian (Le Magoarou et al., 2018) or its eigenspace (Frerix and Bruna, 2019) using sequences of sparse or structured operators, such as Givens rotations or butterfly-like factorizations, aiming to reduce the complexity relative to dense eigendecomposition. However, spectral-mismatch errors with these methods are difficult to control *a priori*, and finding optimal factorizations is NP-hard, which incurs substantial setup costs when compared to our approach, which is quadratic in the number of nodes. While (Fernández-Menduiña et al., 2025) established the link between rank-one updates and spectral graph theory, the resulting factorization of (3) was valid only under some restrictions on the eigenvalues of \mathbf{L} and on the updates. Moreover, the work (Fernández-Menduiña et al., 2025) focused on incremental rank-one updates of path graphs and did not consider the problem of decomposing an arbitrary graph to facilitate the factorization of its GFT.

2.4. Problem statement

We seek to construct spectral operators that compute the GFT of a given graph using efficient localized computations. To this end, we rely on hierarchical decompositions into subgraphs connected by sparse interfaces.

Definition 2.3 (Hierarchical graph family (HGF)). Let $\{\mathcal{G}_i\}_{i=1}^m$ be a collection of base graphs. A graph \mathcal{G} belongs to the hierarchical graph family $\mathcal{F}(L, \{\mathcal{G}_i\}_{i=1}^m, k)$ if it can be constructed by recursively merging pairs of subgraphs over L levels, where at each level at most k edges (bridge edges) are added between any pair of subgraphs.

Clearly, every graph belongs to at least one HGF since we can choose each base graph to be a singleton node and add edges one at a time. By representing a graph as an HGF, we can formalize the algorithmic complexity of the GFT computation. In particular, graphs exhibiting modular or multiscale structure, which are typical in practice (Barthélemy, 2011), admit HGFs with small interface sizes, enabling efficient divide-and-conquer processing.

In this paper, given a graph $\mathcal{G} \in \mathcal{F}(L, \{\mathcal{G}_i\}, k)$, we show that its GFT basis can be factorized into a sequence of Cauchy factors (Theorem 3.1), and we provide an $O(n^2k)$ algorithm to compute this factorization (Theorem 3.2).

Moreover, for arbitrary graphs, we propose algorithms to identify hierarchies that optimize factorization complexity (Section 4). L2G-Net relies on this factorization, yielding a new class of spectral GNNs that avoids $O(n^3)$ eigendecompositions and introduces local inductive biases (Section 5).

3. Cauchy factorization of the GFT

We first generalize the result of (Fernández-Menduiña et al., 2025) to remove the constraints on the eigenvalues and updates (see Section C for details) by introducing *Cauchy factors*, which will play a similar role to the Cauchy matrices in (3) for the case of arbitrary graphs. While we focus on the Laplacian case, the following results hold for any symmetric matrix.

Definition 3.1 (Cauchy factor (CF)). Let \mathcal{S} denote the set of indices corresponding to distinct eigenvalues λ_i such that $\mathbf{z} = \mathbf{U}^\top \mathbf{v}$ has nonzero entries in the associated eigenspaces, and define the symmetric matrix $\tilde{\mathbf{L}} = \mathbf{L} + \rho \mathbf{v} \mathbf{v}^\top$. The associated Cauchy factor is defined as

$$\mathbf{D}(\tilde{\boldsymbol{\lambda}}, \boldsymbol{\lambda}) = \mathbf{P}_\mathcal{S}^\top \begin{bmatrix} \mathbf{I} & \mathbf{0} \\ \mathbf{0} & -\mathbf{C}(\tilde{\boldsymbol{\lambda}}_\mathcal{S}, \boldsymbol{\lambda}_\mathcal{S}) \end{bmatrix} \mathbf{P}_\mathcal{S}, \quad (4)$$

where $\mathbf{C}(\tilde{\boldsymbol{\lambda}}_\mathcal{S}, \boldsymbol{\lambda}_\mathcal{S})$ is an OCLM, \mathbf{I} is the identity on invariant spectral directions of dimension $(n - |\mathcal{S}|)$, and $\mathbf{P}_\mathcal{S}$ permutes the basis so that invariant and affected components are grouped together.

In this case, $\mathbf{C}(\tilde{\boldsymbol{\lambda}}_\mathcal{S}, \boldsymbol{\lambda}_\mathcal{S})$ corresponds to the OCLM associated with the deflated problem. The following result generalizes (Fernández-Menduiña et al., 2025) from path-graph Laplacians to arbitrary symmetric matrices.

Lemma 3.1 (Progressive decomposition identity). *Let $\tilde{\mathbf{L}} = \mathbf{L} + \alpha \mathbf{v} \mathbf{v}^\top = \tilde{\mathbf{U}} \text{diag}(\tilde{\boldsymbol{\lambda}}) \tilde{\mathbf{U}}^\top$, with $\mathbf{L} = \mathbf{U} \text{diag}(\boldsymbol{\lambda}) \mathbf{U}^\top$. Then, generalizing (3), the updated eigenvectors are*

$$\tilde{\mathbf{U}}^\top = \mathbf{D}(\tilde{\boldsymbol{\lambda}}, \boldsymbol{\lambda}) \mathbf{U}^\top. \quad (5)$$

Proof. See Theorem D.1 in the Appendix. \square

We can now extend this identity to HGFs.

Theorem 3.1 (Cauchy factorization). *Let $\mathcal{G} \in \mathcal{F}(L, \{\mathcal{G}_i\}_{i=1}^m, k)$ with Laplacian $\mathbf{L} = \mathbf{U} \text{diag}(\boldsymbol{\lambda}) \mathbf{U}^\top$. Let \mathbf{U}_0 denote the block-diagonal matrix, where each block contains the eigenvectors of one subgraph \mathcal{G}_i . Then,*

$$\mathbf{U}^\top = \mathbf{D}(\boldsymbol{\lambda}, \tilde{\boldsymbol{\lambda}}_{K-1}) \cdots \mathbf{D}(\tilde{\boldsymbol{\lambda}}_1, \tilde{\boldsymbol{\lambda}}_0) \mathbf{U}_0^\top, \quad (6)$$

where $\tilde{\boldsymbol{\lambda}}_0$ are the eigenvalues of the partitioned graph, and $\tilde{\boldsymbol{\lambda}}_\ell$ follows by removing $\ell = 1, \dots, K$ bridge edges from \mathcal{G} , where $K = k(2^L - 1)$.

Algorithm 1 Cauchy factorization

Input: HGF graph $\mathcal{G} \in \mathcal{F}(L, \{\mathcal{G}_i\}_{i=1}^m, k)$.
Output: Eigenvalues λ , Cauchy history \mathcal{H} .

- 1: **1. Initialization**
- 2: Compute leaf eigendecompositions $\{(\mathbf{U}_i, \lambda_i)\}$.
- 3: Initialize set of transformed updates, $\mathcal{Z} = \emptyset$.
- 4: **for** each bridge edge $e = (u, v)$ **do**
- 5: $\mathcal{Z} \leftarrow \mathcal{Z} \cup (\mathbf{e}_u - \mathbf{e}_v)$
- 6: Project all $\mathbf{z} \in \mathcal{Z}$ into the leaf bases \mathbf{U}_i .
- 7: **2. Hierarchical merge**
- 8: **for** level $\ell = 1$ to L **do**
- 9: **for** each pair of subgraphs to merge **do**
- 10: Concatenate eigenvalues: $\lambda \leftarrow [\lambda_L; \lambda_R]$.
- 11: **for** each bridge edge e connecting them **do**
- 12: Retrieve projection vector $\mathbf{z} \in \mathcal{Z}$.
- 13: **Solve** the secular equation to get λ_{new} .
- 14: **Construct** OCLM \mathbf{C} from $(\mathbf{z}, \lambda, \lambda_{\text{new}})$.
- 15: **Update** relevant $\mathbf{z}' \in \mathcal{Z}$ via $\mathbf{z}' \leftarrow \mathbf{C}^\top \mathbf{z}'$.
- 16: $\lambda \leftarrow \lambda_{\text{new}}, \quad \mathcal{H} \leftarrow \mathcal{H} \cup \{\mathbf{C}\}$
- 17: **return** λ, \mathcal{H}

Proof. Sketch: By [Proposition 2.1](#), the Laplacian of \mathcal{G} can be written as a sequence of rank-one edge updates to connect the m subgraphs \mathcal{G}_i . Applying the progressive decomposition identity in [Lemma 3.1](#) to each update and composing the resulting Cauchy factors yields the stated factorization. The full proof is given in [Section D](#). \square

Next, we show that this factorization can be computed in quadratic time in the number of nodes. The following theorem provides the complexity of computing the Cauchy factorization of any member of a hierarchical graph family.

Theorem 3.2. *Let $\mathcal{G} \in \mathcal{F}(L, \{\mathcal{G}_i\}_{i=1}^m, k)$. Assume the eigendecomposition of leaf subgraph \mathcal{G}_i can be computed in $O(f_i(n))$ time. Then, we can find the Cauchy decomposition of the eigenvectors basis of the graph Laplacian \mathbf{L} in $O(kn^2 + \sum_i f_i(n))$ for a sequential solver and $O(kn^2 + \max_i f_i(n))$ for a parallel solver.*

Proof. See [Section E](#). \square

For simplicity, we focus on the parallel case. We highlight two cases: 1) when $L = \log_2 n$, the base graphs become trivial and the complexity is $O(kn^2)$, and 2) when $k \ll n, k = O(1)$, i.e., connections between graphs are sparse, the complexity becomes $O(n^2 + \max_i f_i(n))$. An outline of the algorithm is depicted in [Algorithm 1](#), and the full algorithm is shown in [Algorithm 2](#). Next, we show how to find a suitable HGF (or partition) for a given graph.

4. Finding a suitable HGF

Although every graph admits an HGF decomposition, when $k = O(n)$ the decompositions may not be favorable for computation. We provide a greedy algorithm that, given any graph, partitions it into subgraphs so that the partition minimizes the cost of computing the Cauchy factorization. When decomposition yields diminishing returns, we use spectral sparsification to reduce the interface size.

4.1. Greedy HGF construction

To construct an HGF, based on the GFT factorization cost ([Theorem 3.2](#)) we develop a heuristic that favors balanced partitions with few bridge edges. For a given graph, we generate candidate partitions using balanced cuts with varying balance constraints (e.g., spectral bisection based on the Fiedler vector with varying balance tolerances) ([Ng et al., 2001](#)). To accept a partition, we evaluate whether the split offers computational benefits based on [Theorem 3.2](#). Let $f(\mathcal{G})$ denote the theoretical complexity cost of processing graph \mathcal{G} , i.e., the eigendecomposition complexity. Given a graph \mathcal{G} and a candidate split into subgraphs $\mathcal{G}_1, \mathcal{G}_2$, we accept the partition only if:

$$n^2 k + \max_{i=1,2} f(\mathcal{G}_i) < f(\mathcal{G}). \quad (7)$$

If this condition holds, we recur on \mathcal{G}_1 and \mathcal{G}_2 . If no balanced cut satisfies this condition, we mark the subgraph as a leaf or apply the sparsification strategy below.

Regarding spectral bisection, using the Lanczos algorithm, each iteration requires a matrix-vector multiplication with the Laplacian, which costs $O(|E|)$ time for sparse graphs. The total runtime is therefore $O(|E|T)$, where T is the number of iterations required for convergence. Hence, computing the Fiedler vector is nearly linear in the number of edges and is not a computational bottleneck.

4.2. Interface sparsification

When partitioning fails to reduce the cost function, rather than keeping all edges crossing the cut, we remove some of them via a sparse spectral sparsifier ([Spielman and Srivastava, 2008](#)). We use spectral sparsification in a localized manner, applying the sparsifier to subgraph interfaces.

Theorem 4.1 (Interface sparsification for HGFs). *Let $\mathcal{G} \in \mathcal{F}(L, \{\mathcal{G}_i\}_{i=1}^m, k)$ and $\varepsilon \in (0, 1)$. Then there exists a graph $\mathcal{G}' \in \mathcal{F}(L, \{\mathcal{G}_i\}_{i=1}^m, k')$ such that their combinatorial Laplacians \mathbf{L} and \mathbf{L}' satisfy $\forall \mathbf{x} \in \mathbb{R}^n$,*

$$(1 - \varepsilon) \mathbf{x}^\top \mathbf{L} \mathbf{x} \leq \mathbf{x}^\top \mathbf{L}' \mathbf{x} \leq (1 + \varepsilon) \mathbf{x}^\top \mathbf{L} \mathbf{x}, \quad (8)$$

where $k' \leq O(n \log n / \varepsilon^2)$, and \mathcal{G}' can be constructed in $O(n \log n)$ time using the Spielman–Srivastava sparsifier.

Proof. Fix the hierarchical partition defining \mathcal{G} . At each level, consider the subgraph induced by the bridge edges connecting pairs of subgraphs. Applying spectral sparsification (Spielman and Srivastava, 2008) independently to each such interface yields a graph with at most $k' = O(\varepsilon^{-2})$ edges per interface, while preserving the Laplacian quadratic form within $(1 \pm \varepsilon)$. Since sparsification preserves vertex partition, the resulting graph \mathcal{G}' belongs to the same HGF with reduced interface size. \square

By Theorem 4.1, any graph can be replaced by a spectrally equivalent member of an HGF with bounded interface size, ensuring that the complexity bounds of Theorem 3.2 apply up to a controllable approximation error. From the perspective of Cauchy factorization, sparsification can be viewed as a theoretically grounded form of truncation, limiting the effective number of the Cauchy updates while preserving the Laplacian quadratic form up to a controlled error. One consequence of the result above is that, for spectral filters $g(\cdot)$ that are Lipschitz continuous on the spectrum of \mathbf{L} , the output of a spectral layer based on \mathbf{L}' deviates from that based on \mathbf{L} by at most $O(\varepsilon)$, with the constant depending on the Lipschitz constant of $g(\cdot)$ (Levie et al., 2021).

5. L2G-Net

We describe how L2G-Net can be integrated into a GNN architecture. A conceptual overview is shown in Figure 1b. L2G-Net can be used as a drop-in replacement for standard spectral graph convolution layers, which potentially may involve pointwise non-linearities and residual connections.

Assume a stack of M spectral layers, acting over $\mathbf{X}_0 \in \mathbb{R}^{n \times n_f}$, where n_f is the number of channels. Let $\mathbf{Z}_m = \mathbf{X}_m \mathbf{W}_m$. Then, the c th channel of the output is given by:

$$\mathbf{X}_{m+1,c} = \mathbf{U}g_{\theta,c}(\boldsymbol{\lambda})\mathbf{U}^\top \mathbf{Z}_{m,c}, \quad m = 0, \dots, M - 1. \quad (9)$$

At a high level, our construction modifies the forward transform $\mathbf{U}^\top \mathbf{Z}_{m,c}$ by applying spectral processing independently on small base subgraphs using learnable local graph filters. Then, information is progressively mixed across larger graph components through a sequence of Cauchy factors (cf. Theorem 3.1). Finally, the synthesis transform is computed, again using the same factorization.

We start from the Cauchy factorization in Theorem 3.1. We insert learnable local filters before and after multiplying by the set of Cauchy factors corresponding to the interfaces between each pair of subgraphs. Let these filters be $g_{r,p}(\cdot)$ for the r th level, with $r = 0, \dots, L$, and considering the p th pair of subgraphs, with $p = 1, \dots, 2^r - 1$. Let $\mathbf{D}_{r,p}$ be the product of the Cauchy factors corresponding to the same interface. Given the spectral representations at level

Table 1. Average test accuracy with standard deviation for 10 random train/test partitions on the benchmark in (Platonov et al., 2023). We report the best-performing methods per family. We show average Acc for *Roman-empire* (R. Emp.) and *Amazon-ratings* (Am. Rat.) and AUC for *Tolokers* (Tolok.) and *Minesweeper* (Mines.). Higher is better (\uparrow). See also Table 5.

Method	R. Emp.	Am. Rat.	Mines.	Tolok.
GCN	73.69(0.7)	48.70(0.6)	89.75(0.5)	83.64(0.7)
CO-GNN	91.57(0.3)	54.17(0.4)	97.31(0.4)	84.45(1.2)
Polynormer	92.55 (0.3)	54.81 (0.5)	97.46(0.4)	85.91 (0.7)
MP-SSM	90.91(0.5)	53.65(0.7)	95.33(0.7)	85.26(0.9)
St-ChebNet	92.03(0.9)	53.15(0.2)	95.71(2.3)	85.55(3.4)
Ours	<u>92.12</u> (1.1)	53.41(1.3)	97.50 (0.3)	<u>85.57</u> (0.6)

Table 2. Runtime (s) for computing the eigenvalue decomposition (ED) and the Cauchy factorization (CF) on heterophilous graphs from (Platonov et al., 2023).

Method	R. Emp.	Am. Rat.	Mines.	Tolok.
ED	731.12	896.56	92.34	117.57
CF (ours)	232.49	281.30	32.21	91.33

$r - 1$ on each subgraph, $\mathbf{H}_{p,1}^{r-1}$ and $\mathbf{H}_{p,2}^{r-1}$, we compute:

$$\mathbf{H}_p^{(r)} = g_{r,p}(\boldsymbol{\lambda}_{r,p})\mathbf{D}_{r,p} \begin{bmatrix} \mathbf{H}_{p_1}^{(r-1)} \\ \mathbf{H}_{p_r}^{(r-1)} \end{bmatrix}, \quad (10)$$

where $\boldsymbol{\lambda}_{r,p}$ are the eigenvalues of the merged subgraph at level r . By repeating this procedure recursively up to $r = L$, we obtain the spectral representation $\mathbf{H}^{(L)}$. We will denote by $\mathbf{U}(\Phi)$ the matrix replacing \mathbf{U} with the concatenation of GFTs, filtering, and Cauchy matrices, where Φ represents learnable parameters for all r and p . The output in the node domain is given by $\mathbf{X}_{\text{out}} = \mathbf{U}g_{\theta}(\boldsymbol{\lambda})\mathbf{U}(\Phi)\mathbf{X}_m$. We remark that products by \mathbf{U} are computed using the factorization, so \mathbf{U} is never explicitly computed.

6. Experiments

Our experiments have two goals. First, we validate our theoretical complexity predictions on synthetic graphs with controlled structure. Second, we evaluate the proposed method on real-world graphs that may deviate from the ideal hierarchical setup, including settings requiring aggressive interface sparsification. While our primary contribution is to provide a principled framework for exploiting hierarchical graph structure when it is present, the GNN experiments demonstrate that the approach degrades gracefully under approximation, remaining competitive even with up to 99.5% edge sparsification. All experiments are conducted on an Intel(R) Core(TM) i9-9900K CPU @ 3.60GHz with an NVIDIA GeForce RTX 2070 GPU.

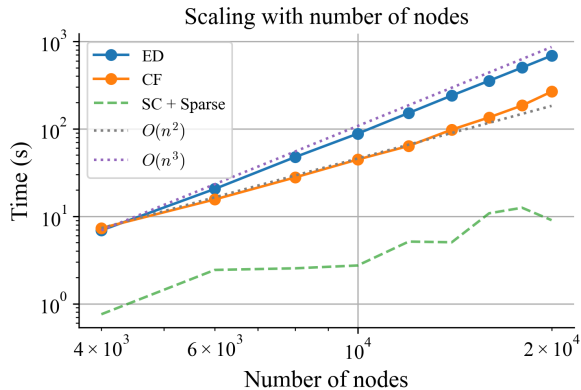


Figure 2. Runtime on a random graph for eigendecomposition (ED), Cauchy factorization (CF), and preprocessing (SC+Sparse). The Cauchy factorization scales quadratically with the number of nodes. The preprocessing time is negligible.

6.1. Synthetic experiments

We validate the predictions of [Theorem 3.2](#) measuring the runtime of the proposed Cauchy factorization on synthetic graphs. We isolate the dependence on graph size and interface size. All experiments are run on the CPU.

Setup. We generate random graphs using the Barabási-Albert model ([Barabási and Albert, 1999](#)). For each graph with n nodes, we first compute a balanced partition using spectral bisection based on the Fiedler vector of the combinatorial Laplacian. We repeat this process again on each subgraph to obtain a partition with 4 subgraphs. The edges crossing the cut define the interface between the two subgraphs. To control the interface size, we sparsify the cut edges, retaining a fixed target number of bridge edges.

Runtime vs graph size (Figure 2). We compare (i) full eigendecomposition of the Laplacian via `numpy.linalg.eigh` and (ii) our Cauchy factorization. We report the median runtime across three runs as a function of the number of nodes n for a fixed interface size $k = 5$. Eigendecomposition scales with $O(n^3)$ and becomes impractical beyond $n \approx 10^4$. In contrast, the proposed Cauchy factorization follows a clear quadratic trend, consistent with the $O(kn^2)$ complexity predicted by our analysis. As n increases, the cost of the base eigendecompositions of the individual subgraphs becomes non-negligible, causing the overall trend to gradually approach cubic behavior. This effect is expected and can be mitigated by increasing the number of partitions; when the number of levels is $L = \log n$, the base graphs have $O(1)$ nodes, making the complexity of the base eigendecompositions trivial. [Figure 2](#) shows that the preprocessing overhead (spectral cut and sparsification) remains negligible across all graph sizes considered.

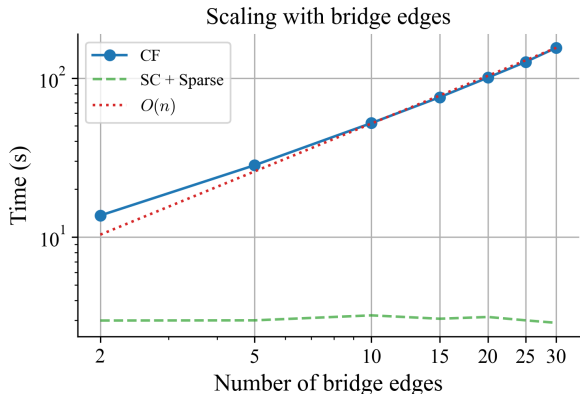


Figure 3. Runtime as a function of k on a random graph for Cauchy factorization (CF) and preprocessing (SC+Sparse). The complexity of the Cauchy factorization scales linearly with the interface size. The preprocessing time is negligible and roughly constant with k .

Runtime vs. cut size (Figure 3). For a fixed graph size ($n = 8000$), the runtime of the proposed Cauchy factorization grows linearly with the number of crossing edges, k , which corresponds to the number of the Cauchy updates. This confirms that the computational cost is governed by the interface size rather than by the total graph size. The preprocessing step based on spectral cuts and sparsification exhibits an approximately constant runtime, as promised by [Theorem 4.1](#). These results show that our method remains efficient because you can sparsify first to reduce the interface size and this sparsification has limited complexity.

6.2. Real-world graphs

Setup. We evaluate the proposed method on a heterophilous benchmark suite ([Platonov et al., 2023](#)), which comprises large-scale graphs designed to challenge locality-based MPNNs. In particular, we focus on *Roman-Empire*, *Amazon-Ratings*, *Minesweeper*, and *Tolokers*. These datasets combine non-local dependencies with graph sizes for which the global GFT remains feasible but is very slow, making them particularly well-suited for assessing our approach. Although our experiments focus on transductive setups, our approach is as expressive as classical spectral GNNs and compatible with their inductive use cases. We rely on the normalized Laplacian, although we sparsify based on the combinatorial Laplacian. We use either splines or radial basis functions with learnable centers. We ensure that the filters in each filter bank sum to one over the spectrum ([Wang and Zhang, 2022](#)). Our method first partitions the graph into two subgraphs (one level of hierarchy) and sparsifies the cut. A single shared filter is used across all feature channels and layers (cf. [Section B](#)).

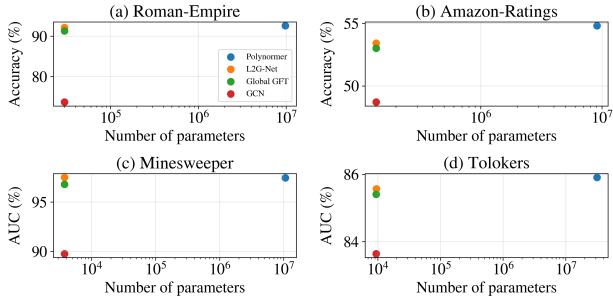


Figure 4. Performance vs complexity comparison. L2G-Net achieves competitive or superior performance with orders of magnitude fewer learnable parameters than state-of-the-art baselines, and outperforms the Global GFT across all datasets.

Performance (Table 1). L2G-Net achieves competitive or superior performance across all benchmarks, exceeding the best baselines (Deng et al., 2024) on *Minesweeper* and remaining close to the strongest methods on the others. Notably, while attention-based models such as Polynormer attain strong accuracy, they do so at the cost of learned graph structures that are harder to interpret (cf. Figure 5).

Runtime (Table 2). We report the computational cost of CF and the eigendecomposition. CF yields substantial speedups across all datasets. We highlight the performance in *Tolokers* as a worst-case scenario: this graph is particularly dense, so the number of edges between subgraphs remains high after sparsification. Even in this case, we obtain runtime gains over direct eigendecomposition.

Learnable parameters (Figure 4). We compare Global GFT, L2G-Net, and Polynormer across the four datasets. The topological inductive bias allows L2G-Net to compete with state-of-the-art methods while using orders of magnitude fewer learnable parameters. Moreover, L2G-Net consistently outperforms the Global GFT baseline across all datasets, highlighting the benefit of localized spectral processing over fully global spectral representations.

6.3. Local processing

Setup. To analyze the localization of predictive importance across graph nodes, we perform a node-level attribution study using Grad-CAM (Selvaraju et al., 2017) on the *Minesweeper* dataset. For each evaluation sample, we compute Grad-CAM scores at the node level, normalize them to sum to one, and sort nodes by decreasing importance. We then compute the cumulative sum of importance as a function of the fraction of nodes retained, yielding a cumulative contribution curve per sample. These curves are finally averaged across the evaluation set; confidence intervals are reported, but remain very small and are visually negligible.

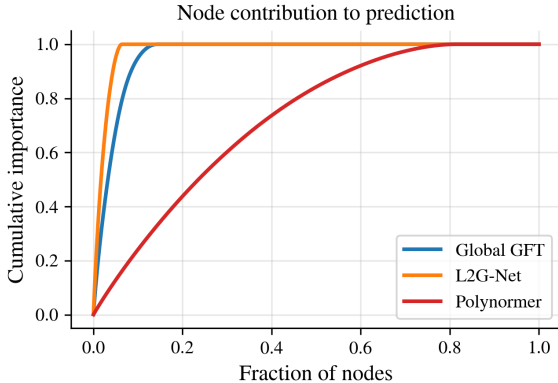


Figure 5. Cumulative node contribution to the prediction on *Minesweeper*. Average across validation set; shaded areas indicate confidence intervals. L2G-Net localizes predictive power on a smaller fraction of nodes than Global GFT. The node contributions of Polynormer are less localized in the original graph.

Results (Figure 5). L2G-Net concentrates its predictive contributions on a small subset of nodes, reflecting its local bias. The Global GFT baseline spreads importance over a larger portion of the graph, consistent with global spectral representations. For Polynormer (Deng et al., 2024), graph learning combined with attention-based mechanisms leads to more diffuse contributions, making explanations difficult to interpret with respect to the input geometry.

7. Conclusion

We introduced an exact factorization of the GFT for arbitrary graphs based on Cauchy matrices and graph partitions. This factorization enables a divide-and-conquer strategy for spectral processing, reducing the cost of exact GFT-based operators from $O(n^3)$ to $O(n^2)$, scaled by the subgraph interface size. We proposed an algorithm to find partitions that minimize the factorization cost and, when this remains costly, reduce complexity via interface sparsification, allowing adaptation to arbitrary graph topologies. Building on these results, we introduced L2G-Net, a new class of spectral GNNs that combine local and global spectral processing by construction. L2G-Net is most appropriate in regimes where long-range dependencies are essential and polynomial filters would require high order or deep architectures, leading to oversquashing or numerical instability. Experiments on synthetic and real-world benchmarks serve to validate the theoretical analysis, confirming the predicted runtime scaling and demonstrating that the resulting models remain competitive while requiring significantly fewer parameters than transformer-based methods and lower preprocessing cost than global spectral methods. The proposed factorization framework opens new directions for fast and structured spectral algorithms on graphs.

References

- Uri Alon and Eran Yahav. On the bottleneck of graph neural networks and its practical implications. *arXiv preprint arXiv:2006.05205*, 2020.
- Álvaro Arroyo, Alessio Gravina, Benjamin Gutteridge, Federico Barbero, Claudio Gallicchio, Xiaowen Dong, Michael Bronstein, and Pierre Vandergheynst. On vanishing gradients, over-smoothing, and over-squashing in gnn: Bridging recurrent and graph learning. *arXiv preprint arXiv:2502.10818*, 2025.
- Albert-László Barabási and Réka Albert. Emergence of scaling in random networks. *science*, 286(5439):509–512, 1999.
- Federico Barbero, Ameya Velingker, Amin Saberi, Michael Bronstein, and Francesco Di Giovanni. Locality-aware graph-rewiring in gnn. *arXiv preprint arXiv:2310.01668*, 2023.
- Marc Barthélemy. Spatial networks. *Physics reports*, 499(1-3):1–101, 2011.
- Joshua Batson, Daniel A Spielman, and Nikhil Srivastava. Twice-Ramanujan sparsifiers. *SIAM Rev.*, 56(2):315–334, 2014.
- Michael M. Bronstein, Joan Bruna, Yann LeCun, Arthur Szlam, and Pierre Vandergheynst. Geometric deep learning: Going beyond euclidean data. *IEEE Signal Process. Mag.*, 34(4):18–42, 2017. doi: 10.1109/MSP.2017.2693418.
- Joan Bruna, Wojciech Zaremba, Arthur Szlam, and Yann Lecun. Spectral networks and locally connected networks on graphs. In *International Conference on Learning Representations (ICLR2014)*, CBLS, April 2014, pages http–openreview, 2014.
- James R. Bunch, Christopher P. Nielsen, and Danny C. Sorensen. Rank-one modification of the symmetric eigenproblem. *Numerische Mathematik*, 31:31–48, 1978.
- Difeng Cai, Edmond Chow, Lucas Erlandson, Yousef Saad, and Yuanzhe Xi. Smash: Structured matrix approximation by separation and hierarchy. *Numerical Linear Algebra with Applications*, 25(6), 2018. doi: <https://doi.org/10.1002/nla>.
- Ben Chamberlain, James Rowbottom, Maria I Gorinova, Michael Bronstein, Stefan Webb, and Emanuele Rossi. Grand: Graph neural diffusion. In *International conference on machine learning*, pages 1407–1418. PMLR, 2021.
- Ming Chen, Zhewei Wei, Zengfeng Huang, Bolin Ding, and Yaliang Li. Simple and deep graph convolutional networks. In *International Conference on Machine Learning (ICML)*, 2020.
- Fan RK Chung. *Spectral graph theory*, volume 92. American Mathematical Soc., 1997.
- Aaron Clauset, Cristopher Moore, and M. E. J. Newman. Hierarchical structure and the prediction of missing links in networks. *Nature*, 453(7191):98–101, 2008. doi: 10.1038/nature06830.
- Carl de Boor. *A Practical Guide to Splines*. Springer, revised edition edition, 2001.
- Michaël Defferrard, Xavier Bresson, and Pierre Vandergheynst. Convolutional neural networks on graphs with fast localized spectral filtering. *Advances in neural information processing systems*, 29, 2016.
- Chenhui Deng, Zichao Yue, and Zhiru Zhang. Polynormer: Polynomial-expressive graph transformer in linear time. *arXiv preprint arXiv:2403.01232*, 2024.
- Vijay Prakash Dwivedi and Xavier Bresson. A generalization of transformer networks to graphs. *arXiv preprint arXiv:2012.09699*, 2020.
- Vijay Prakash Dwivedi, Ladislav Rampásek, Michael Galkin, Ali Parviz, Guy Wolf, Anh Tuan Luu, and Dominique Beaini. Long range graph benchmark. *Advances in Neural Information Processing Systems*, 35: 22326–22340, 2022.
- Dario Fasino. Orthogonal Cauchy-like matrices. *Numerical Algorithms*, 92(1):619–637, 2023.
- Samuel Fernández-Menduiña, Eduardo Pavez, and Antonio Ortega. Fast DCT+: A family of fast transforms based on rank-one updates of the path graph. In *Proc. IEEE Int. Conf. Acoust., Speech, and Signal Process.* IEEE, 2025.
- Thomas Frerix and Joan Bruna. Approximating orthogonal matrices with effective givens factorization. In *Intl. Conf. on Mach. Learn.*, pages 1993–2001. PMLR, 2019.
- N Gastinel. Inversion d’une matrice generalisant la matrice de Hilbert. *Chiffres*, 3:149–152, 1960.
- Gene H Golub. Some modified matrix eigenvalue problems. *SIAM Rev.*, 15(2):318–334, 1973.
- Ming Gu and Stanley C. Eisenstat. Efficient algorithms for computing a strong rank-revealing qr factorization. *SIAM Journal on Scientific Computing*, 17(4):848–869, 1996. doi: 10.1137/0917055. URL <https://doi.org/10.1137/0917055>.

- Ali Hariri, Álvaro Arroyo, Alessio Gravina, Moshe Eliasof, Carola-Bibiane Schönlieb, Davide Bacciu, Kamyar Aizzadenesheli, Xiaowen Dong, and Pierre Vandergheynst. Return of chebnet: Understanding and improving an overlooked gnn on long range tasks. *arXiv preprint arXiv:2506.07624*, 2025.
- Mingguo He, Zhewei Wei, Hongteng Xu, et al. Bernnet: Learning arbitrary graph spectral filters via bernstein approximation. *Advances in neural information processing systems*, 34:14239–14251, 2021.
- Yinan Huang, William Lu, Joshua Robinson, Yu Yang, Muhan Zhang, Stefanie Jegelka, and Pan Li. On the stability of expressive positional encodings for graphs. *arXiv preprint arXiv:2310.02579*, 2023.
- Laurent Jacques. A quantized johnson–lindenstrauss lemma: The finding of buffon’s needle. *IEEE Transactions on Information Theory*, 61(9):5012–5027, 2015.
- Thomas N Kipf and Max Welling. Semi-supervised classification with graph convolutional networks. In *International Conference on Learning Representations*, 2017.
- Luc Le Magoarou, Rémi Gribonval, and Nicolas Tremblay. Approximate fast graph fourier transforms via multilayer sparse approximations. *IEEE Trans on Sign. and Inform. Process. over Netw.*, 4(2):407–420, 2018. doi: 10.1109/TSIPN.2017.2710619.
- Ron Levie, Federico Monti, Xavier Bresson, and Michael M Bronstein. Cayleynets: Graph convolutional neural networks with complex rational spectral filters. *IEEE Transactions on Signal Processing*, 67(1):97–109, 2018.
- Ron Levie, Wei Huang, Lorenzo Bucci, Michael Bronstein, and Gitta Kutyniok. Transferability of spectral graph convolutional neural networks. *Journal of Machine Learning Research*, 22(272):1–59, 2021.
- Guohao Li, Matthias Müller, Ali Thabet, and Bernard Ghanem. Deepgens: Can gens go as deep as cnns? In *2019 IEEE/CVF International Conference on Computer Vision (ICCV)*, pages 9266–9275, 2019. doi: 10.1109/ICCV.2019.00936.
- Ren-Cang Li. Solving secular equations stably and efficiently. Technical Report UCB/CSD-94-851, Dec 1994. URL <http://www2.eecs.berkeley.edu/Pubs/TechRpts/1994/5882.html>.
- Andrew Ng, Michael Jordan, and Yair Weiss. On spectral clustering: Analysis and an algorithm. In T. Dietterich, S. Becker, and Z. Ghahramani, editors, *Proc. Advan. Neural Inf. Process. Syst.*, volume 14. MIT Press, 2001.
- Antonio Ortega, Pascal Frossard, Jelena Kovačević, José MF Moura, and Pierre Vandergheynst. Graph signal processing: Overview, challenges, and applications. *Proc. IEEE*, 106(5):808–828, 2018.
- Victor Y Pan. *Structured matrices and polynomials: unified superfast algorithms*. Springer Science & Business Media, 2012.
- Oleg Platonov, Denis Kuznedelev, Michael Diskin, Artem Babenko, and Liudmila Prokhorenkova. A critical look at the evaluation of gnns under heterophily: Are we really making progress? *arXiv preprint arXiv:2302.11640*, 2023.
- Michael Poli, Stefano Massaroli, Junyoung Park, Atsushi Yamashita, Hajime Asama, and Jinkyoo Park. Graph neural ordinary differential equations. *arXiv preprint arXiv:1911.07532*, 2019.
- Michael JD Powell. Radial basis functions for multivariable interpolation: a review. *Algorithms for approximation*, pages 143–167, 1987.
- T Konstantin Rusch, Michael M Bronstein, and Siddhartha Mishra. A survey on oversmoothing in graph neural networks. *arXiv preprint arXiv:2303.10993*, 2023.
- Ramprasaath R Selvaraju, Michael Cogswell, Abhishek Das, Ramakrishna Vedantam, Devi Parikh, and Dhruv Batra. Grad-cam: Visual explanations from deep networks via gradient-based localization. In *Proceedings of the IEEE international conference on computer vision*, pages 618–626, 2017.
- Daniel A Spielman and Nikhil Srivastava. Graph sparsification by effective resistances. In *Proceedings of the fortieth annual ACM symposium on Theory of computing*, pages 563–568, 2008.
- Xiyuan Wang and Muhan Zhang. How powerful are spectral graph neural networks. In *International conference on machine learning*, pages 23341–23362. PMLR, 2022.

Supplementary Materials

A. Further definitions and notations

This section formalizes conventions and assumptions that are used throughout the paper but may be implicit in the main exposition.

Secular equation

Secular equations yield the eigenvalues of the system after a rank-one update, based on the eigenvalues of the matrix being updated and the update itself.

Proposition A.1 (Secular equation, (Golub, 1973)). *Let $\mathbf{L} = \mathbf{U}\text{diag}(\boldsymbol{\lambda})\mathbf{U}^\top$ and $\tilde{\mathbf{L}} = \mathbf{L} + \rho \mathbf{v}\mathbf{v}^\top = \tilde{\mathbf{U}}\text{diag}(\tilde{\boldsymbol{\lambda}})\tilde{\mathbf{U}}^\top$. Then each $\tilde{\lambda}_j$ satisfies*

$$1 + \rho \sum_{i=1}^n z_i^2 / (\tilde{\lambda}_j - \lambda_i) = 0, \quad (11)$$

where $\mathbf{z} = \mathbf{U}^\top \mathbf{v}$.

Eigenvalues before and after the update satisfy an interleaving property (Golub, 1973). In practice, we use Li’s secular equation solver (Li, 1994).

Proposition A.2 (Eigenvalue interleaving (Bunch et al., 1978)). *Provided $\rho > 0$, the eigenvalues after the update satisfy:*

$$\lambda_1 \leq \tilde{\lambda}_1 \leq \lambda_2 \leq \dots \leq \lambda_n \leq \tilde{\lambda}_n. \quad (12)$$

This result guarantees that we can solve the secular equation efficiently (Gu and Eisenstat, 1996).

Laplacian conventions

We consider weighted undirected graphs with adjacency matrix \mathbf{W} and self-loop matrix $\mathbf{V} \succeq 0$. The generalized graph Laplacian (GGL) is defined as

$$\mathbf{L} \doteq \mathbf{D} - \mathbf{W} + \mathbf{V}, \quad (13)$$

where $\mathbf{D} = \text{diag}(\mathbf{1}^\top \mathbf{W})$ is the degree matrix. Unless otherwise stated, all theoretical results are derived for the combinatorial Laplacian \mathbf{L} .

In experiments, we consider the normalized Laplacian

$$\mathbf{L}_{\text{norm}} \doteq \mathbf{D}^{-1/2} \mathbf{L} \mathbf{D}^{-1/2}, \quad (14)$$

whose eigenvectors are orthonormal under the standard Euclidean inner product. All spectral factorizations apply identically after normalization, up to a change of basis induced by $\mathbf{D}^{-1/2}$.

Eigenvalue ordering and degeneracies

Let $\mathbf{L} = \mathbf{U}\text{diag}(\boldsymbol{\lambda})\mathbf{U}^\top$ denote an eigendecomposition of a symmetric Laplacian matrix. Eigenvalues are assumed to be sorted in non-decreasing order. In the presence of repeated eigenvalues, the corresponding eigenvectors are not unique; any orthonormal basis spanning the eigenspace is valid.

When rank-one updates leave certain eigenspaces invariant, we apply deflation (Section C) to isolate the affected subspace. This operation preserves orthogonality and does not alter the asymptotic complexity of the factorization.

Affected spectral indices

Given a rank-one update $\tilde{\mathbf{L}} = \mathbf{L} + \rho \mathbf{v} \mathbf{v}^\top$ with $\mathbf{L} = \mathbf{U} \text{diag}(\boldsymbol{\lambda}) \mathbf{U}^\top$, define the projection vector

$$\mathbf{z} = \mathbf{U}^\top \mathbf{v}. \quad (15)$$

When \mathbf{L} has distinct eigenvalues, we define the set of affected spectral indices as

$$\mathcal{S} \doteq \{i \mid z_i \neq 0\}. \quad (16)$$

When \mathbf{L} has repeated eigenvalues, the associated eigenspaces are not uniquely defined. In this case, we exploit the rotational freedom within each eigenspace and choose an orthonormal eigenbasis such that, for each eigenspace, at most one basis vector has a nonzero projection onto \mathbf{v} (Bunch et al., 1978). This choice is always possible and leaves the eigendecomposition of \mathbf{L} unchanged. The definition of \mathcal{S} then applies unchanged, with \mathbf{U} denoting the chosen eigenbasis.

Only eigenpairs indexed by \mathcal{S} are modified by the rank-one update; eigenvectors corresponding to indices outside \mathcal{S} remain invariant. For bridge edges connecting two subgraphs, \mathcal{S} is restricted to spectral components associated with those subgraphs, yielding localized Cauchy factors.

Rank-one versus rank- k updates

Each individual edge insertion corresponds to a rank-one update of the Laplacian. Interfaces consisting of k bridge edges therefore induce a sequence of k rank-one updates, each associated with its own Cauchy factor. The resulting transformation is given by the product of these factors, yielding a rank- k modification of the spectrum.

All theoretical results are stated for rank-one updates and extend directly to rank- k interfaces by composition.

Spectral locality

We say that a linear operator $\mathbf{A} \in \mathbb{R}^{n \times n}$ is s -local in the spectral domain if it acts non-trivially on at most s spectral coordinates, i.e., if

$$\mathbf{A} = \mathbf{P}^\top \begin{bmatrix} \mathbf{I}_{n-s} & \mathbf{0} \\ \mathbf{0} & \mathbf{B} \end{bmatrix} \mathbf{P}, \quad (17)$$

for some permutation matrix \mathbf{P} and $\mathbf{B} \in \mathbb{R}^{s \times s}$.

Cauchy factors induced by bridge edges are $O(|V_i| + |V_j|)$ -local, where V_i and V_j are the vertex sets of the connected subgraphs. In contrast, the full GFT basis is n -local. This distinction underpins the locality–globality trade-off exploited by L2G-Net.

Non-uniqueness of hierarchical decompositions

The hierarchical graph family (HGF) decomposition of a graph is generally not unique. Different choices of partitions and merge orders yield different factorizations with identical spectral semantics. Our objective is not to recover a unique hierarchy, but to identify decompositions that minimize computational cost while preserving spectral equivalence.

Graph sparsification

Graph sparsification seeks to approximate a graph \mathcal{G} with a sparser graph $\tilde{\mathcal{G}}$ whose Laplacian remains spectrally close to that of \mathcal{G} . Let \mathbf{L} and $\tilde{\mathbf{L}}$ denote the corresponding graph Laplacians. A $(1 \pm \varepsilon)$ spectral sparsifier satisfies

$$(1 - \varepsilon) \mathbf{x}^\top \mathbf{L} \mathbf{x} \leq \mathbf{x}^\top \tilde{\mathbf{L}} \mathbf{x} \leq (1 + \varepsilon) \mathbf{x}^\top \mathbf{L} \mathbf{x}, \quad \forall \mathbf{x} \in \mathbb{R}^n.$$

such a sparsifier can be constructed by sampling edges proportionally to their effective resistances, yielding $\tilde{\mathcal{G}}$ with $O(n \log n / \varepsilon^2)$ edges and preserving the spectrum of \mathbf{L} up to relative error (Spielman and Srivastava, 2008). In this work, we use spectral sparsification in a localized manner, applying these guarantees to inter-subgraph interfaces. This reduces the number of connecting edges while preserving the quadratic form of the global Laplacian.

Table 3. Dataset-specific hyperparameter settings for L2G-Net.

Dataset	d	Layers	K	Banks (G/S/T)	Basis	Dropout	LR	Steps	Sparsif.
<i>Roman-Empire</i>	64	5	8	4 / 1 / 1	Spline	0.25	2×10^{-4}	1000	0.005
<i>Amazon-Ratings</i>	256	4	6	1 / 1 / 1	Spline	0.30	4×10^{-3}	1500	0.005
<i>Minesweeper</i>	32	14	6	6 / 1 / 1	Spline	0.225	2×10^{-3}	1000	0.005
<i>Tolokers</i>	64	3	4	1 / 1 / 1	RBF	0.20	8×10^{-4}	2000	0.01

B. Experimental details

The hyperparameters reported in Table 3 specify the architectural, spectral, and optimization settings used for L2G-Net across datasets.

The hidden dimension d denotes the dimensionality of node embeddings throughout the network. *Layers* corresponds to the number of stacked blocks, each consisting of a spectral filtering stage followed by a shared feed-forward module with residual connections. The parameter K denotes the number of spectral filters per filter bank, which determines the resolution at which the graph spectrum is sampled.

Banks (G/S/T) specifies the number of filter banks used for the global spectrum (G) and for the two partitioned subgraphs induced by the graph cut (S and T), respectively. Using multiple banks allows the model to represent a richer family of spectral responses while maintaining parameter sharing across layers.

Basis indicates the type of spectral basis used to parameterize the filters. For most datasets, filters are expressed using B-spline bases defined over the normalized Laplacian eigenvalues, which encourage smooth spectral responses. For *Tolokers*, we instead use a radial basis function (RBF) parameterization with learnable centers and widths, which empirically provides greater flexibility on highly irregular spectra.

Dropout denotes the feature dropout probability applied to node representations during training. *LR* is the base learning rate used by the AdamW optimizer. *Steps* denotes the total number of optimization steps performed during training.

Finally, *Sparsif.* refers to the interface sparsification ratio used during graph partitioning. In particular, in practice, we can interpret the parameter as using $\max(1, \text{edges after}/\text{edges before} * 100)$ edges. This parameter controls the fraction of cut edges retained via effective resistance sampling, trading off computational cost and approximation accuracy in the spectral decomposition. A higher value retains more edges across the partition boundary, while smaller values lead to more aggressive sparsification.

Cross-partition edges are sparsified using resistance-based sampling. The partition is obtained via a Fiedler vector computed with LOBPCG ($k=2$, 40 iterations), using a quantile sweep over $[0.45, 0.55]$. Effective resistances are approximated with a JL (Jacques, 2015) with dimension $k = \lceil 24 \log |V| / \varepsilon^2 \rceil$ using $\varepsilon = 0.5$, with a minimum of $k = 20$. Crossing edges are sampled with replacement according to probabilities proportional to $w_e \tilde{R}_e$, where \tilde{R}_e is the approximate resistance. A fraction ρ of crossing edges is retained, depending on the dataset, and sampled edges are reweighted by $(qp_e)^{-1}$. For details regarding the performance of the sparsifier, we refer the reader to (Spielman and Srivastava, 2008).

B.1. Base layer formulation

Following (Hariri et al., 2025), we adopt an ODE-inspired formulation. Let $\mathbf{X}(t)$ denote the node features at continuous time t . We let $\mathbf{U}(\Phi)$ be the local-to-global forward transform with local filtering in our method. Then,

$$d\mathbf{X}(t) = \mathbf{U}g_\theta(\boldsymbol{\lambda})\mathbf{U}(\Phi)^\top \mathbf{X}(t)\mathbf{W} dt. \quad (18)$$

Applying an explicit Euler discretization with step size $\epsilon > 0$ yields the update for layer $m = 0, \dots, M - 1$:

$$\mathbf{X}_{m+1} = \mathbf{X}_m + \epsilon \mathbf{U}g_\theta(\boldsymbol{\lambda})\mathbf{U}(\Phi)^\top \mathbf{X}_m \mathbf{W}. \quad (19)$$

Depth allows for compositionality (learning complex non-linearities) rather than to expand the receptive field, which is already global due to the spectral formulation. Unlike (Hariri et al., 2025), the complexity of the spectral filter does not directly control the norm of the layer Jacobian in our model. To reduce the parameter count, we share \mathbf{W} and the spectral filter parameters θ, Φ across layers. Furthermore, we also share the spectral filter across channels.

Table 4. Statistics of real-world heterophilous graph datasets from Platonov *et al.* (Platonov *et al.*, 2023).

Dataset	Nodes	Edges	Avg. Degree	Features	Classes	k after sparse
<i>Roman-empire</i>	22,662	32,927	2.91	300	18	1
<i>Amazon-ratings</i>	24,492	93,050	7.60	300	5	1
<i>Minesweeper</i>	10,000	39,402	7.88	7	2	1
<i>Tolokers</i>	11,758	519,000	88.28	10	2	25

B.2. Learnable spectral filter centers

We allow each spectral filter to be a linear combination of basis functions whose centers are learned jointly with the model:

$$g_\theta(\boldsymbol{\lambda}) = \mathbf{B}(\boldsymbol{\lambda}; \boldsymbol{\mu})\boldsymbol{\alpha}, \quad (20)$$

where $\mathbf{B}(\boldsymbol{\lambda}; \boldsymbol{\mu}) \in \mathbb{R}^{n \times K}$ is a basis matrix (e.g., radial basis functions (Powell, 1987) or splines (de Boor, 2001)) evaluated at learnable centers $\boldsymbol{\mu} \in [0, 1]^K$, and $\boldsymbol{\alpha}$ are trainable coefficients. By learning the centers $\boldsymbol{\mu}$, the model can place spectral support where it is most useful for the task.

B.3. Real-world graph properties

We provide some information about the properties of the graphs we consider in Table 4. We also include the interface size after sparsification during our experiments.

C. Deflation

The derivation in (Fernández-Menduiña *et al.*, 2025), which is generalized in our work, assumes a worst-case scenario¹ where 1) the GGL before the rank-one update has no repeated eigenvalues and 2) the rank-one update used to add an edge is not orthogonal to any element in the original bases of the eigenspace. In these cases, we first deflate the matrix, reducing the computational complexity of the factorization. Following (Bunch *et al.*, 1978), consider the rank-one update:

$$\tilde{\mathbf{L}} = \mathbf{L} + \rho \mathbf{v}\mathbf{v}^\top = \tilde{\mathbf{U}}\text{diag}(\tilde{\boldsymbol{\lambda}})\tilde{\mathbf{U}}^\top \quad (21)$$

where $\mathbf{L} = \mathbf{U}\text{diag}(\boldsymbol{\lambda})\mathbf{U}^\top$ is the original eigendecomposition. Let $\mathbf{z} = \mathbf{U}^\top \mathbf{v}$ be the projection of the perturbation vector onto the eigenspace of \mathbf{L} . Then, we can write: $\tilde{\mathbf{L}} = \mathbf{U}(\text{diag}(\boldsymbol{\lambda}) + \rho \mathbf{z}\mathbf{z}^\top)\mathbf{U}^\top$. The idea of deflation is that, in some scenarios, we can find a set of eigenvectors of \mathbf{L} (potentially different than \mathbf{U}) such that some of its elements are orthogonal to the original rank-one update \mathbf{v} , so that \mathbf{z} has some zero entries. Since \mathbf{U} in our case is given by our algorithm, we differentiate two cases: direct deflation (case 1) and deflation after applying a Householder reflector (case 2).

Case 1: Zero components ($z_i = 0$, for $i = 1, \dots, \ell$). The perturbation is then orthogonal to the basis of the original eigenspace. We obtain $\tilde{\lambda}_i = \lambda_i$ and $\tilde{\mathbf{u}}_i = \mathbf{u}_i$:

$$\tilde{\mathbf{L}}\mathbf{u}_i = \mathbf{U}(\text{diag}(\boldsymbol{\lambda}) + \rho \mathbf{z}\mathbf{z}^\top)\mathbf{e}_i = \mathbf{U}(\text{diag}(\boldsymbol{\lambda})\mathbf{e}_i) = \lambda_i \mathbf{u}_i, \quad (22)$$

where \mathbf{e}_i is the i th element of the canonical basis.

Deflation: Remove column and row i from $(\text{diag}(\boldsymbol{\lambda}) + \rho \mathbf{z}\mathbf{z}^\top)$. Construct the Cauchy matrix based on the updated secular equation. During multiplication, let $\mathbf{u}_i^\top \mathbf{x}$ be the i th coefficient, i.e., let it pass through unmodified.

Effect on complexity: Reduces the problem size from n to $n - \ell$, where ℓ is the number of zero components.

Case 2: Repeated eigenvalues. Consider a repeated eigenvalue λ_k with multiplicity m , and let $\mathcal{S}_k = \{i : \lambda_i = \lambda_k\}$ denote the index set of all eigenvectors corresponding to λ_k . The basis for this eigenspace is not unique; any orthogonal transformation of $\{\mathbf{u}_i\}_{i \in \mathcal{S}_k}$ yields another valid basis. We can exploit this freedom to choose a new basis that zeroes out components of \mathbf{z} . Let \mathbf{z}_k be the m -dimensional subvector of \mathbf{z} corresponding to the indices in \mathcal{S}_k . We can find an $m \times m$

¹Worst case in terms of complexity: applying deflation simplifies the factorization.

orthogonal matrix \mathbf{Q} (e.g., a Householder reflector) such that:

$$\mathbf{Q}^\top \mathbf{z}_k = \|\mathbf{z}_k\|_2 \mathbf{e}_1. \quad (23)$$

Applying this rotation to the basis of the eigenspace results in a new set of eigenvectors where the transformed perturbation vector, $\hat{\mathbf{z}}$, has $m - 1$ zero components in the subspace. Since the eigenvalues are identical within this subspace ($\lambda_i = \lambda_k \forall i \in \mathcal{S}_k$), the diagonal matrix $\text{diag}(\boldsymbol{\lambda})$ is invariant under this rotation. This effectively reduces the problem to Case 1 for $m - 1$ eigenpairs, as they become orthogonal to the perturbation.

Deflation: Construct an orthogonal matrix \mathbf{Q} that transforms the subvector \mathbf{z}_k as shown above. Let $\hat{\mathbf{U}} = \mathbf{U}_{\mathcal{S}_k} \mathbf{Q}$. This rotation leaves $m - 1$ eigenpairs, $(\lambda_k, \hat{\mathbf{u}}_j)$, unaffected by the rank-one update. We can then remove the $m - 1$ rows and columns of $(\text{diag}(\boldsymbol{\lambda}) + \rho \hat{\mathbf{z}} \hat{\mathbf{z}}^\top)$ corresponding to the positions where $\hat{\mathbf{z}}$ is zero and solve the smaller problem.

Effect on complexity: Reduces the problem size from n to $n - (m - 1)$.

D. Proof of Theorem 3.1

We show that the Laplacian eigenvectors of any graph in $\mathcal{F}(L, \{\mathcal{G}_i\}_{i=1}^m, k)$ can be written as a chain product of CF. We denote by \mathbf{x}_i the subset of \mathbf{x} corresponding to the subset of nodes of \mathcal{G} represented by \mathcal{G}_i .

D.1. CF decomposition

First, we establish the following property of any GGL, which states that the Laplacian decomposes into rank-one updates, one for each edge contribution.

Proposition D.1 ((Batson et al., 2014)). *Let \mathbf{e}_j be the j th canonical vector, for $j = 1, \dots, n$. Then, the GGL \mathbf{L} of an undirected graph can be written as*

$$\mathbf{L} = \sum_{(i,j) \in \mathcal{E}, i \neq j} w_{ij} (\mathbf{e}_i - \mathbf{e}_j)(\mathbf{e}_i - \mathbf{e}_j)^\top + \sum_{(i,i) \in \mathcal{E}} w_{ii} \mathbf{e}_i \mathbf{e}_i^\top, \quad (24)$$

where w_{ij} denotes the edge weights, for $i, j = 1, \dots, |\mathcal{V}|$.

We can state now the following result, which generalizes (Fernández-Menduiña et al., 2025) to arbitrary symmetric matrices.

Theorem D.1 (Progressive decomposition identity). *The eigenvector basis $\tilde{\mathbf{U}}^\top$ of $\tilde{\mathbf{L}} = \tilde{\mathbf{U}} \text{diag}(\tilde{\boldsymbol{\lambda}}) \tilde{\mathbf{U}}^\top = \mathbf{L} + \alpha \mathbf{v} \mathbf{v}^\top$, with $\mathbf{L} = \mathbf{U} \text{diag}(\boldsymbol{\lambda}) \mathbf{U}^\top$, decomposes as*

$$\tilde{\mathbf{U}}^\top = -\mathbf{D}(\tilde{\boldsymbol{\lambda}}, \boldsymbol{\lambda}) \mathbf{U}^\top. \quad (25)$$

Proof. When \mathcal{S} is empty, the result boils down to the progressive factorization in (Fernández-Menduiña et al., 2025). When \mathcal{S} is not empty, we apply deflation first, and construct $\mathbf{C}(\boldsymbol{\lambda}_{\mathcal{S}}, \boldsymbol{\lambda}_{\mathcal{S}})$ from the deflated matrix. \square

When $\tilde{\mathbf{L}}$ is the Laplacian of a graph, this result offers a *progressive factorization* of the Laplacian eigenvectors: we can decompose the new basis as the eigenvectors of the unperturbed Laplacian multiplied by a CF.

Then, we can design a decomposition that starts with a fully disconnected graph and progressively adds edges. Let $\lambda_0, \dots, \lambda_{|\mathcal{E}|}$ be the sequence of eigenvalues of the GGL of the graph obtained by performing each step of this process. Then, we can state the following result.

Lemma D.1 (CF decomposition). *The Laplacian eigenvectors of the GGL $\mathbf{L} = \mathbf{U} \text{diag}(\boldsymbol{\lambda}) \mathbf{U}^\top$ of any graph \mathcal{G} can be written as the product of $|\mathcal{E}|$ CF:*

$$\mathbf{U}^\top = \mathbf{D}(\lambda_{|\mathcal{E}|}, \lambda_{|\mathcal{E}|-1}) \dots \mathbf{D}(\lambda_2, \lambda_1) \mathbf{D}(\lambda_1, \lambda_0). \quad (26)$$

Proof. The result follows from applying Theorem D.1 accounting for every possible rank-one update in Proposition 2.1. \square

Now, we can use the previous result to state a decomposition for graphs in $\mathcal{F}(L, \{\mathcal{G}_i\}_{i=1}^m, k)$. We define the stack of matrices of base transforms as:

$$\mathbf{U}_b^\top \doteq \begin{bmatrix} \mathbf{U}_1^\top & \mathbf{0} & \dots & \mathbf{0} \\ \mathbf{0} & \mathbf{U}_2^\top & \dots & \mathbf{0} \\ \vdots & \ddots & \ddots & \vdots \\ \mathbf{0} & \mathbf{0} & \dots & \mathbf{U}_m^\top \end{bmatrix}. \quad (27)$$

Let λ be the eigenvalues of the GGL for the graph with the isolated base components. We then denote by $\tilde{\lambda}_i$, for $i = 1, \dots, k(2^L - 1)$, the eigenvalues resulting from each rank-one update.

Lemma D.2 (HGF decomposition). *Let $\tilde{\mathbf{U}}$ be Laplacian eigenvectors of any graph $\mathcal{G} \in \mathcal{F}(L, \{\mathcal{G}_i\}_{i=1}^m, k)$. Then,*

$$\tilde{\mathbf{U}}^\top = \mathbf{D}(\tilde{\lambda}_{k(2^L-1)}, \tilde{\lambda}_{k(2^L-1)-1}) \dots \mathbf{D}(\tilde{\lambda}_1, \lambda) \mathbf{U}_b^\top. \quad (28)$$

Proof. The result follows by induction from [Proposition 2.1](#) and [Theorem D.1](#). \square

Although the decomposition consists of $k(2^L - 1)$ products, in a HGF each CF modifies only a reduced subset of the input vector, which can be exploited to systematically reduce complexity. The next result shows that CF are localized only to the subgraphs they modify.

Proposition D.2 (Edge connection). *Consider a graph \mathcal{G} with GGL \mathbf{L} formed by a set of m disconnected subgraphs \mathcal{G}_i , for $i = 1, \dots, m$. Let $\tilde{\mathbf{L}} \in \mathcal{P}_1(\mathbf{L})$ and $n = |\mathcal{V}|$. Then,*

$$\mathbf{D}(\tilde{\lambda}, \lambda) = \mathbf{P}_S^\top \begin{bmatrix} \mathbf{I}_{n-s \times n-s} & \mathbf{0} \\ \mathbf{0} & -\mathbf{C}(\tilde{\lambda}_S, \lambda_S) \end{bmatrix} \mathbf{P}_S \in \mathbb{R}^{n \times n}. \quad (29)$$

with

- $s = |\mathcal{V}_i| + |\mathcal{V}_j|$ when the rank-one update connects \mathcal{G}_i to \mathcal{G}_j , with $i \neq j$,
- $s = |\mathcal{V}_i|$ when the rank-one update affects only the subgraph \mathcal{G}_i .

Proof. [Section D.2](#). \square

The previous result states that when we join two distinct subgraphs \mathcal{G}_i and \mathcal{G}_j via a rank-one update, the corresponding CF is an identity matrix except for a block of size $s = |\mathcal{V}_i| + |\mathcal{V}_j|$. This localizes the update to only the dimensions corresponding to the vertices of those two subgraphs. In the next section, we provide a method to implement these structured matrix products efficiently.

D.2. Proof of the edge-connect lemma

Proof. From the progressive property [Theorem D.1](#) and the definition of CF, we have to show that the transform version of the rank-one update $\mathbf{U}_b^\top \mathbf{v}$ has at least $n - s$ zeros. Since

$$\mathbf{z} = \mathbf{U}_b^\top \mathbf{v} = \begin{bmatrix} \mathbf{U}_1^\top & \mathbf{0} & \dots & \mathbf{0} \\ \mathbf{0} & \mathbf{U}_2^\top & \dots & \mathbf{0} \\ \vdots & \ddots & \ddots & \vdots \\ \mathbf{0} & \mathbf{0} & \dots & \mathbf{U}_m^\top \end{bmatrix} \mathbf{v} = \begin{bmatrix} \mathbf{U}_1^\top \mathbf{v}_1 \\ \mathbf{U}_2^\top \mathbf{v}_2 \\ \vdots \\ \mathbf{U}_m^\top \mathbf{v}_m \end{bmatrix}, \quad (30)$$

where \mathbf{v}_i denotes the subsection of the vector \mathbf{v} that corresponds to the i th subgraph. Now, for the first case, \mathbf{v} only has two non-zero components, which will be in \mathbf{v}_i and \mathbf{v}_j . Therefore, $\mathbf{U}_k^\top \mathbf{v}_k$ is zero for all $k \neq i, j$. This set comprises $n - s$ components, with $s = |\mathcal{V}_i| + |\mathcal{V}_j|$. Therefore, the first result follows.

For the second case, both non-zero components will lie in \mathbf{v}_i . Therefore, $\mathbf{U}_k^\top \mathbf{v}_k$ is zero for all $k \neq i$. This set comprises $n - s$ components, with $s = |\mathcal{V}_i|$. Therefore, the result follows. \square

E. Transform setup

We detail our algorithm for eigendecomposition in [Algorithm 2](#). We analyze its complexity as follows:

- **Apply transform.** Since we add k edges between pairs of subgraphs, the maximum number of edges touching any given subgraph is kL . Therefore, for a matrix $\mathbf{M} \in \mathbb{R}^{s \times s}$, the complexity of each call is

$$O(g(s)kL),$$

where $g(s)$ is the complexity of the matrix-vector product with the input matrix. This bound is a worst-case bound over the full hierarchy; tighter level-wise bounds are used in the merging analysis

- **Initialization.** Creating and updating each element of \mathcal{Z} is linear in the size of the smallest graphs, $n/2^L$. Since we have at most $k \sum_{\ell=1}^L 2^{L-\ell} = k(2^L - 1)$ elements in \mathcal{Z} , the cost is upper bounded by $O(nk)$.

The eigendecomposition of the leaf graphs has cost

$$O\left(\sum_{i=1}^m f_i(n)\right).$$

Updating all elements of \mathcal{Z} across all levels requires

$$k(2^L - 1)O(n/2^L) = O(kn).$$

While we are multiplying by dense matrices, multiplying by each element of the canonical basis amounts to selecting the corresponding column of the dense matrix. Since we have to scale by the weight, the complexity becomes $2n/2^L$, which yields the result.

- **Hierarchical merging.** Solving the secular equation at level ℓ costs $O((n/2^{L-\ell})^2)$. Since at that level, at most $k 2^{L-\ell}$ edges participate, this operation has complexity

$$\sum_{\ell=1}^L k 2^{L-\ell} O((n/2^{L-\ell})^2) = O(kn^2).$$

We must also apply the corresponding Cauchy updates. The complexity of an update is $O(g(n/2^{L-\ell})kL)$ per edge, since each edge update requires a multiplication by all the other existing updates that touch the corresponding subgraph. Therefore the total merging complexity is

$$\sum_{\ell=1}^L k 2^{L-\ell} O(kLg(n/2^{L-\ell})) = O\left(k^2L \sum_{\ell=1}^L g(n/2^{L-\ell})2^{L-\ell}\right).$$

Since $g(n) = n \log n$ ([Pan, 2012](#)), we reach

$$O(kn^2 + k^2n(L^2 \log n - L^3)).$$

Thus, the full complexity of the algorithm is

$$O\left(kn^2 + \sum_{i=1}^m f_i(n)\right)$$

Parallel solver. Under parallel execution:

- **Initialization.** Since each block operates on disjoint edges in \mathcal{Z} , all operations can be carried out in parallel. The complexity becomes

$$O\left(\max_{i=1, \dots, m} f_i(n)\right).$$

- **Hierarchical merging.** All subgraph pairs at level ℓ are independent, so the work at that level parallelizes fully. The work on each level is still governed by the cost of solving the secular equation, which has to be solved sequentially. Therefore, the complexity remains $O(kn^2)$.

Thus, the parallel version has complexity

$$O\left(kn^2 + \max_{i=1,\dots,m} f_i(n)\right).$$

F. MORE EXPERIMENTAL RESULTS

In [Table 5](#), we compare our method with a benchmark based on [\(Platonov et al., 2023\)](#).

Algorithm 2 Cauchy factorization

Input:

- 1: Hierarchical graph $\mathcal{G} \in \mathcal{F}(L, \{\mathcal{G}_i\}_{i=1}^m, k)$
- 2: Bridge edge sets $\mathcal{E}_{\ell,i}$ with corresponding weights $w(\cdot)$ for $i = 1, \dots, 2^{L-\ell}$ and levels $\ell = 1 \dots L$.

Output:

- 3: Final eigenvalues $\lambda \in \mathbb{R}^N$, Cauchy rotation history $\mathcal{H} = \{\mathcal{H}_1, \dots, \mathcal{H}_L\}$.

```

4: function ApplyTransform( $\mathcal{I}, \mathbf{M}, \mathcal{Z}$ )
5:    $\mathcal{E}_{\text{act}} \leftarrow \{e = (u, v) \in \text{Keys}(\mathcal{Z}) \mid \{u, v\} \cap \mathcal{I} \neq \emptyset\}$  ▷ Update edge vectors touching node set  $\mathcal{I}$ 
6:   for each  $e \in \mathcal{E}_{\text{act}}$ 
7:      $\mathbf{z}_{\text{loc}} \leftarrow \text{Extract}(\mathcal{Z}[e], \mathcal{I})$ 
8:      $\mathcal{Z}[e] \leftarrow \text{Insert}(\mathcal{Z}[e], \mathbf{M}^\top \mathbf{z}_{\text{loc}})$ 
9:   return  $\mathcal{Z}$ 
    
```

10: 1. Initialization step

- ```

11: $\mathcal{E}_{\text{total}} \leftarrow \bigcup_{\ell,i} \mathcal{E}_{\ell,i}$
12: Initialize \mathcal{Z} as map: edge \mapsto sparse length- N vector
13: for each $e = (u, v) \in \mathcal{E}_{\text{total}}$ do
14: $\mathcal{Z}[e] \leftarrow \sqrt{w(e)} (\mathbf{e}_u - \mathbf{e}_v)$
15: $\mathcal{S}_{\text{curr}} \leftarrow$ empty list
16: for $i = 1 \dots m$
17: $(\mathbf{U}_i, \lambda_i) \leftarrow \text{DENSEEIGSLAP}(\mathcal{G}_i)$
18: $\mathcal{I}_i \leftarrow$ sorted node set of leaf \mathcal{G}_i
19: $\mathcal{Z} \leftarrow \text{APPLYTRANSFORM}(\mathcal{I}_i, \mathbf{U}_i, \mathcal{Z})$
20: Append $(\lambda_i, \mathcal{I}_i)$ to $\mathcal{S}_{\text{curr}}$

```

**20: 2. Hierarchical merging**

- ```

21: for  $\ell = 1 \dots L$  do
22:    $\mathcal{S}_{\text{next}} \leftarrow$  empty list
23:    $\mathcal{H}_\ell \leftarrow \emptyset$ 
24:   for  $i = 1 \dots |\mathcal{S}_{\text{curr}}|/2$  do
25:     Retrieve left  $(\lambda_A, \mathcal{I}_A) \leftarrow \mathcal{S}_{\text{curr}}[2i - 1]$ 
26:     Retrieve right  $(\lambda_B, \mathcal{I}_B) \leftarrow \mathcal{S}_{\text{curr}}[2i]$ 
27:      $\mathcal{I}_{\text{new}} \leftarrow \mathcal{I}_A \cup \mathcal{I}_B$ 
28:      $\lambda_{\text{new}} \leftarrow [\lambda_A; \lambda_B]$ 
29:     for each bridge  $e \in \mathcal{E}_{\ell,k}$  do
30:        $\mathbf{z} \leftarrow \text{Extract}(\mathcal{Z}[e], \mathcal{I}_{\text{new}})$ 
31:        $(\lambda_{\text{new}}, \mathbf{C}) \leftarrow \text{SOLVESECULAR}(\lambda_{\text{new}}, \mathbf{z})$ 
32:        $\mathcal{Z} \leftarrow \text{APPLYTRANSFORM}(\mathcal{I}_{\text{new}}, \mathbf{C}, \mathcal{Z})$ 
33:        $\mathcal{H}_\ell \leftarrow \mathcal{H}_\ell \cup \{\mathbf{C}\}$ 
34:     Append  $(\lambda_{\text{new}}, \mathcal{I}_{\text{new}})$  to  $\mathcal{S}_{\text{next}}$ 
35:    $\mathcal{S}_{\text{curr}} \leftarrow \mathcal{S}_{\text{next}}$ 
    
```

- 36: **return** final λ from $\mathcal{S}_{\text{curr}}$ and \mathcal{H}

Algorithm 3 Solve secular Equation

Input:

- 1: Old eigenvalues $\lambda = (\lambda_1, \dots, \lambda_n)$, sorted ascending
- 2: Projection vector $\mathbf{z} \in \mathbb{R}^n$

Output:

- 3: Updated eigenvalues $\tilde{\lambda}$
 - 4: Cauchy matrix $\mathbf{C} \in \mathbb{R}^{n \times n}$ (columns are eigenvectors)
 - 5: **function** SOLVESECULAR(λ, \mathbf{z})
 - 6: $n \leftarrow \text{length}(\lambda)$
 - 7: Initialize $\tilde{\lambda} \in \mathbb{R}^n$
 - 8: **for** $j = 1 \dots n$ **do**
 - 9: Solve for $\tilde{\lambda}_j$ in $(\lambda_j, \lambda_{j+1})$: $1 + \sum_{k=1}^n z_k^2 / (\tilde{\lambda}_j - \lambda_k) = 0$
 - 10: Initialize $\mathbf{C} \in \mathbb{R}^{n \times n}$
 - 11: **for** $j = 1 \dots n$ **do** ▷ For each new eigenvalue (Column)
 - 12: **for** $i = 1 \dots n$ **do** ▷ For each component (Row)
 - 13: $C_{ij} \leftarrow z_i / (\tilde{\lambda}_j - \lambda_i)$
 - 14: Normalize column j : $\mathbf{C}_{:,j} \leftarrow \mathbf{C}_{:,j} / \|\mathbf{C}_{:,j}\|_2$
 - 15: **return** $\tilde{\lambda}, \mathbf{C}$
-

Table 5. Performance comparison on long-range benchmarks. Results are reported as mean \pm standard deviation. We report Acc for *Roman-empire* and *Amazon-ratings* and AUC for *Tolokers* and *Minesweeper*. Higher is better (\uparrow). Best method appears in boldface, second best method underlined, third best method in italics.

Model	Roman-empire	Amazon-ratings	Minesweeper	Tolokers
<i>MPNNs</i>				
GAT	80.87 \pm 0.30	49.09 \pm 0.63	92.01 \pm 0.68	83.70 \pm 0.47
GAT (LapPE)	84.80 \pm 0.46	44.90 \pm 0.73	93.50 \pm 0.54	84.99 \pm 0.54
GAT (RWSE)	86.62 \pm 0.53	48.58 \pm 0.41	92.53 \pm 0.65	85.02 \pm 0.67
Gated-GCN	74.46 \pm 0.54	43.00 \pm 0.32	87.54 \pm 1.22	77.31 \pm 1.14
GCN	73.69 \pm 0.74	48.70 \pm 0.63	89.75 \pm 0.52	83.64 \pm 0.67
GCN (LapPE)	83.37 \pm 0.55	44.35 \pm 0.36	94.26 \pm 0.49	84.95 \pm 0.78
GCN (RWSE)	84.84 \pm 0.55	46.40 \pm 0.55	93.84 \pm 0.48	85.11 \pm 0.77
CO-GNN (Σ , Σ)	91.57 \pm 0.32	51.28 \pm 0.56	95.09 \pm 1.18	83.36 \pm 0.89
CO-GNN (μ , μ)	91.37 \pm 0.35	<u>54.17\pm0.37</u>	97.31 \pm 0.41	84.45 \pm 1.17
SAGE	85.74 \pm 0.67	53.63 \pm 0.39	93.51 \pm 0.57	82.43 \pm 0.44
<i>Graph Transformers</i>				
Expformer	89.03 \pm 0.37	53.51 \pm 0.46	90.74 \pm 0.53	83.77 \pm 0.78
NAGphormer	74.34 \pm 0.77	51.26 \pm 0.72	84.19 \pm 0.66	78.32 \pm 0.95
GOAT	71.59 \pm 1.25	44.61 \pm 0.50	81.09 \pm 1.02	83.11 \pm 1.04
GPS	82.00 \pm 0.61	53.10 \pm 0.42	90.63 \pm 0.67	83.71 \pm 0.48
GPSGCN+Performer (LapPE)	83.96 \pm 0.53	48.20 \pm 0.67	93.85 \pm 0.41	84.72 \pm 0.77
GPSGCN+Performer (RWSE)	84.72 \pm 0.65	48.08 \pm 0.85	92.88 \pm 0.50	84.81 \pm 0.86
GPSGCN+Transformer (LapPE)	OOM	OOM	91.82 \pm 0.41	83.51 \pm 0.93
GPSGCN+Transformer (RWSE)	OOM	OOM	91.17 \pm 0.51	83.53 \pm 1.06
GT	86.51 \pm 0.73	51.17 \pm 0.66	91.85 \pm 0.76	83.23 \pm 0.64
GT-sep	87.32 \pm 0.39	52.18 \pm 0.80	92.29 \pm 0.47	82.52 \pm 0.92
Polynormer	92.55\pm0.30	54.81\pm0.49	<u>97.46\pm0.36</u>	<u>85.91\pm0.74</u>
<i>Heterophily-Designated GNNs</i>				
CPGNN	63.96 \pm 0.62	39.79 \pm 0.77	52.03 \pm 5.46	73.36 \pm 1.01
FAGCN	65.22 \pm 0.56	44.12 \pm 0.30	88.17 \pm 0.73	77.75 \pm 1.05
FSGNN	79.92 \pm 0.56	52.74 \pm 0.83	90.08 \pm 0.70	82.76 \pm 0.61
GBK-GNN	74.57 \pm 0.47	45.98 \pm 0.71	90.85 \pm 0.58	81.01 \pm 0.67
GloGNN	59.63 \pm 0.69	36.89 \pm 0.14	51.08 \pm 1.23	73.39 \pm 1.17
GPR-GNN	64.85 \pm 0.27	44.88 \pm 0.34	86.24 \pm 0.61	72.94 \pm 0.97
H2GCN	60.11 \pm 0.52	36.47 \pm 0.23	89.71 \pm 0.31	73.35 \pm 1.01
JacobiConv	71.14 \pm 0.42	43.55 \pm 0.48	89.66 \pm 0.40	68.66 \pm 0.65
<i>Graph SSMs</i>				
GMN	87.69 \pm 0.50	<i>54.07\pm0.31</i>	91.01 \pm 0.23	84.52 \pm 0.21
GPS + Mamba	83.10 \pm 0.28	45.13 \pm 0.97	89.93 \pm 0.54	83.70 \pm 1.05
GRAMA _{GCN}	88.61 \pm 0.43	53.48 \pm 0.62	95.27 \pm 0.71	86.23\pm1.10
MP-SSM	90.91 \pm 0.48	53.65 \pm 0.71	95.33 \pm 0.72	85.26 \pm 0.93
<i>Spectral</i>				
Stable-ChebNet	92.03 \pm 0.85	53.15 \pm 0.21	95.71 \pm 2.26	85.55 \pm 3.35
Ours	<u>92.12\pm1.12</u>	53.41 \pm 1.34	97.50\pm0.26	<i>85.57\pm0.61</i>